PFC/JA-95-45

X-ray Observations of 2l - nl' Transitions from Zr, Nb, Mo and Pd in Near Neonlike Charge States

J.E. Rice, K.B. Fournier[1], J.L. Terry, M.A. Graf,
M. Finkenthal[2], E.S. Marmar, W.H. Goldstein[1]

November, 1995

[1]Lawrence Livermore National Laboratory, Livermore, CA 94550.
[2]Racah Institute of Physics, The Hebrew University, Jerusalem, Israel, 91904.

Submitted to Phys. Rev. A.

This work was supported by the U. S. Department of Energy Contract No. DE-AC02-78ET51013. Reproduction, translation, publication, use and disposal, in whole or in part by or for the United States government is permitted.

X-ray Observations of 2l - nl′ Transitions from Zr, Nb, Mo and Pd in Near Neonlike Charge States

J. E. Rice, K. B. Fournier[+], J. L. Terry, M. A. Graf, M. Finkenthal[!],
E. S. Marmar and W. H. Goldstein[+]

Plasma Fusion Center, MIT, Cambridge, MA 02139-4307

[+] *Lawrence Livermore National Laboratory, Livermore, CA 94550*

[!] *Racah Institute of Physics, The Hebrew University, Jerusalem, Israel, 91904*

Abstract

X-ray spectra of $2l$ - nl' transitions with $3 \leq n \leq 12$ in the row five transition metals zirconium (Z=40), niobium (Z=41), molybdenum (Z=42) and palladium (Z=46) from charge states around neonlike have been observed from Alcator C-Mod plasmas. Accurate wavelengths (± .2 mÅ) have been determined by comparison with neighboring argon, chlorine and sulphur lines with well known wavelengths. Line identifications have been made by comparison to *ab initio* atomic structure calculations, using a fully relativistic, parametric potential code. For neonlike ions, calculated wavelengths and oscillator strengths are presented for 2p-nd transitions with n between 3 and 12. The magnitude of the configuration interaction between the $(2p^5)_{\frac{1}{2}}6d_{\frac{3}{2}}$ $J = 1$ level and the $(2p^5)_{\frac{3}{2}}7d_{\frac{5}{2}}$ $J = 1$ levels has been measured as a function of energy level spacing for successive atomic number neonlike ions, and the agreement with theory is good. Transitions in the $2p_{\frac{1}{2}}$-$nd_{\frac{3}{2}}$ series in neonlike Mo^{32+} with $n \geq 13$ are not observed; the upper levels lie above the first ionization potential of the neonlike ion and have a large branching ratio towards autoionization. Measured and calculated wavelengths and oscillator strengths of selected transitions in the aluminum-, magnesium-, sodium-, fluorine- and oxygenlike isosequences are also presented.

Introduction

Recently there has been considerable interest in x-ray transitions in high Z atoms with charge states around the neonlike isosequence[1-10]. X-ray lasing[11,12] has been demonstrated in neonlike ions, and a need to understand the kinetics of this system has motivated development of very precise collisional-radiative modelling tools[13]. The identifications of many x-ray lines from neonlike ions allow high resolution experimental data to be used for benchmarking multi-electron atomic structure calculations[14-18]. Most of the work which has been done in the past has been limited to 3-3, 2-3 and 2-4 transitions in the Ne-I isosequence and adjacent charge states. The high temperature, optically thin tokamak plasmas enable the measurement of many lines originating in transitions from levels having $n \geq 5$; in fact, all of the transitions in the 2p-nd series in Mo^{32+} lying under the ionization potential have been measured[10]. The availability of a large number of transitions in several adjacent elements provides the opportunity to study the systematics of configuration interaction effects. Also, it has been observed that a systematic uncertainty enters the calculation for the wavelengths of the transitions with a 2s hole in the upper state through the treatment of QED contributions in the calculation of these level energies when a relativistic parametric potential code (RELAC[19,20]) is used. The tendancy to overestimate level energies in multi-electron atoms based on hydrogenic calculations with QED corrections[21] has been noted in comparisons between precise measurements of the level structure in neonlike ytterbium[14] and other relativistic codes which use the same procedure as RELAC. Issues relating to the calculation of level energies for states with a 2s hole have been investigated based on observations of the level structure of neonlike gold[15].

In this paper are presented measured wavelengths and calculated wavelengths and oscillator strengths for 2p-nd transitions with n between 3 and 12 in neonlike Zr, Nb and Pd; 2s-np transitions with n between 3 and 9 in neonlike Zr, Nb, Mo and Pd; fluorinelike 2p-nd transitions with n between 4 and 7 in Zr and Nb and with n between 7 and 10 in Mo; 2p-nd transitions with n between 3 and 7 in sodium- and

magnesiumlike Zr, Nb and Pd; 2p-3d and 2p-4d transitions in aluminumlike Pd; and 2p-4d transitions in oxygenlike Mo, obtained from Alcator C-Mod plasmas[22]. The magnitude of the configuration interaction between the $(2p^5)_{\frac{1}{2}}6d_{\frac{3}{2}}$ $J = 1$ level and the $(2p^5)_{\frac{3}{2}}7d_{\frac{5}{2}}$ $J = 1$ levels has been measured as a function of energy level spacing for successive atomic number neonlike ions, and the agreement with theory is good. Transitions in the $2p_{\frac{1}{2}}$-$nd_{\frac{3}{2}}$ series in neonlike Mo^{32+} with $n \geq 13$ are not observed; the upper levels lie above the first ionization potential of the neonlike ion and have a large branching ratio towards autoionization.

Experiment Description

The x-ray observations described here were obtained from the Alcator C-Mod[22] tokamak, a compact high field device with all molybdenum plasma facing components. For these measurements, the plasma parameters were in the range of 7.7 x $10^{13}/cm^3 \leq n_{e0} \leq 2.0$ x $10^{14}/cm^3$ and 1500 eV $\leq T_{e0} \leq$ 3400 eV. A laser blow-off impurity injection system[23], which has been used to study impurity transport, was used to inject niobium, palladium and zirconium into Alcator C-Mod plasmas.

The spectra presented here were recorded by a five chord, independently spatially scannable, high resolution x-ray spectrometer array[24]. In the present paper, high resolution x-ray observations in the wavelength range 2.84 Å$\leq \lambda \leq$ 4.08 Å are shown. Wavelength calibration[2,3] has been achieved by determining the instrumental dispersions in reference to H- and He-like argon, chlorine and sulphur lines and previously measured molybdenum[10] lines. The argon was introduced through a piezo-electric valve and chlorine is an intrinsic impurity from solvents used to clean vacuum components. Presumably sulphur is a trace impurity in the molybdenum. Lines from hydrogen[25,26]- and heliumlike[27–29] charge states are taken to have well known wavelengths, either measured or calculated.

Calculation of Energy Levels and Oscillator Strengths

Ab initio atomic structure calculations for the aluminum- through oxygenlike isosequences (ground states $2p^6 3s^2 3p$ to $2s^2 2p^4$, respectively) have been performed using the RELAC code[19,20], which solves the Dirac equation by optimizing a parametric potental. Contributions to level energies from the Breit operator and vacuum polarization effects[30] are also computed. RELAC computes the self-energy of a bound electron due to the emission and re-absorption of a virtual photon, in the case of an s- or p-orbital, by computing an effective-Z and interpolating on the hydrogenic values tabulated in Ref.(21). The effective-Z is found by the requirement that the mean value of the relativistic subshell $< r_{nlj} >$ agrees with the corresponding hydrogenic value. RELAC has been used to calculate the full multiconfiguration transition wavelengths and oscillator strengths for all lines observed in this paper. In a previous paper discussing the structure of neonlike molybdenum ions[10], part of the systematically larger difference between observed and calculated 2s-np transition energies, and the more accurately predicted 2p-nd transition energies was ascribed to RELAC's use of the effective-Z method for QED corrections to the binding energies of L-shell electrons. Recent work looking at the energies of $2p^5 3s$ levels in several neonlike ions[17] with atomic numbers from 10 to 90 and the energies of 2s-2p transitions in neonlike uranium[18] implies that a many-body perturbation calculation of the ionic structure of the neonlike ions in the present work can remove most remaining discrepancies between the predicted and observed level energies. A quantitative discussion of the observed and calculated 2s-2p neonlike transition energies will be given below.

This paper presents the wavelengths and oscillator strengths for newly identified 2s-np, 2p-nd and 2p-ns transitions in highly ionized zirconium, niobium, molybdenum and palladium. The 2p-nd transitions considered here are strongly split by the j-value (in jj-coupling) of the 2p hole in the ionic core. The splitting is very apparent in the neonlike ions, where the resonance transitions with upper states containing a $2p_{\frac{1}{2}}$ hole are at much shorter wavelengths than the corresponding transitions with a $2p_{\frac{3}{2}}$ hole. This splitting can lead to significant configuration

interaction when a $(2p^5)_{\frac{1}{2}}$nd orbital is close in energy to a $(2p^5)_{\frac{3}{2}}$n'd (n'>n) orbital. Interaction between the orbitals will perturb transition wavelengths and redistribute oscillator strength within a class of transitions[31]. Another by-product of the above mentioned $2p_j$-splitting in the neonlike series is the possibility of autoionization from the (higher energy) $2p_{\frac{1}{2}}$-$nd_{\frac{3}{2}}$ transitions' upper states. Indeed, for n $\geq$ 12, the upper state of the transition lies above the ground state of the fluorinelike ion, $2s^22p^5$ $J = \frac{3}{2}$, and hence, lines in this series can be quenched by autoionization. RELAC is used to compute the autoionization rate coefficents for this class of transitions in the distorted wave approximation[32]. This quenching effect will be discussed in more detail below.

Experimental Spectra

Shown in Fig.1 are the time histories of several quantities of interest for a typical Alcator C-Mod 6.4 T, deuterium discharge. There was a palladium injection into this particular discharge at 0.5 seconds, when the plasma current was 0.8 MA, the central electron temperature was 2000 eV and the central electron density was 1.5 x $10^{14}/cm^3$. The palladium stayed in the plasma for about 100 ms, as shown by the bottom frame of the figure. In Fig.2 is shown the spectrum taken during an injection which demonstrates the strongest palladium line which falls within the wavelength range of the spectrometer, the $2p^6$ - $(2p^5)_{\frac{3}{2}}3d_{\frac{5}{2}}$ transition in neonlike Pd^{36+} at 3904.7 mÅ. Also apparent in this spectrum are some sodiumlike 2p-3d lines around 3.93 Å, a strong 2p-3d magnesiumlike line at 3948.9 mÅ, several 2p-3d transitions in aluminumlike palladium around 3.98 Å, and a 2p-3s Pd^{36+} line at 4001.4 mÅ. A synthetic spectrum, generated using calculated wavelengths, typical instrumental and Doppler line widths, and line amplitudes proportional to the oscillator strengths within a given charge state, is shown at the bottom of the figure. Wavelength calibration was obtained from several nearby Ar^{16+} lines[28,33], S^{14+} lines[28,29] and S^{15+} lines[25]. The observed palladium lines are within 1 mÅ of the calculated wavelengths (except for the aluminumlike palladium lines, which are

discussed below).

A strong neonlike Nb^{31+} line, the $2p^6$ - $(2p^5)_{\frac{3}{2}}5d_{\frac{5}{2}}$ transition at 3591.2 mÅ, obtained from a niobium injection, is shown in Fig.3. Also prominent in the figure are the 2s-4p Nb^{31+} lines at 3640.5 and 3652.6 mÅ. Sodium and magnesiumlike 2p-5d transitions are apparent, in addition to the $2p^6$ - $(2p^5)_{\frac{1}{2}}4d_{\frac{3}{2}}$ transition in Mo^{32+} at 3626.1 mÅ[10]. The wavelength calibration for this spectrum was obtained from nearby molybdenum[10] and Cl^{15+} lines[28]. At the bottom of the figure is a synthetic spectrum. The wavelength agreement is very good, except in the case of transitions with a 2s hole, as has been discussed elsewhere for molybdenum[10]. Line identifications for several charge states of interest for injected niobium, zirconium and palladium are given in Tables I-VI, where transition upper levels, measured and theoretical wavelengths and calculated oscillator strengths are presented. Complete tables for molybdenum can be found in Ref.(10). Table I summarizes the strongest lines observed, the 2p-nd transitions in the neonlike ions Zr^{30+}, Nb^{31+} and Pd^{36+}. The 2-3 transitions in these ions may be compared with the observations and calculations in Ref.(4). Theoretical wavelengths are within 1 mÅ, or .03% of the observed level energies, and often the calculations are within 0.5 mÅ.

The 2s-np transitions for Zr^{30+}, Nb^{31+}, Mo^{32+} and Pd^{36+} are given in Table II. Theoretical wavelengths for the 2s-np transitions are generally $\sim$2 mÅ shorter than the observed wavelengths. In the case of Pd^{36+}, RELAC predicts that the Lamb shift (vacuum polarization energy[30] and the electron self-energy) to the transition energies will contribute a total of -2.938 and -2.882eV to the 2s-$3p_{\frac{1}{2}}$ and 2s-$3p_{\frac{3}{2}}$ transition energies, respectively; these QED effects increase the calculated transition wavelengths for these two lines by 3.10 and 2.96 mÅ, respectively. (Note, the calculated contribution of the QED effects to the transition energies are less than 0.1% of the total energies). The calculated transition wavelengths are 2.3 and 2.2 mÅ shorter, respectively, than the observed 2s-$3p_{\frac{1}{2}}$ and 2s-$3p_{\frac{3}{2}}$ transition wavelengths. Hence, if all the difference between the calculated and observed transition wavelengths were due to the effective-Z calculation of the electron self-energy,

then RELAC would be over-estimating the nuclear screening (under-estimating the electron self energy) by $\sim$ 70%. The work in Ref. (14) with neonlike Yb^{60+} concludes that the effective-Z approach under-estimates the self-energy contribution (over-estimates nuclear screening effects) to 2s-3p transition energies by $\sim$ 10%. Ytterbium and even heavier neonlike ions[15], are in a regime where the effect of the finite size of the atomic nucleus is not negligible; the effect of the nuclear size on calculated level energies is almost non-existant in elements near in atomic number to paladium. Even so, a 70% under-estimate of the electron self energy by RELAC for the ions in this work is unlikely, so other sources of uncertainty in the theoretical wavelengths in Table II, such as relativistic correlation effects, are being investigated. The measured wavelengths presented here are accurate to $\pm$ .2 mÅ, so these shifts are too large to be instrumental in origin.

For the electron temperature range of Alcator C-Mod, zirconium and niobium can easily reach the fluorinelike state, and several of these transitions are listed in Table III. Many of these observed lines are unresolved blends. (F-like barium 2-3 transitions are presented in Ref.(6).) Sodiumlike and magnesiumlike E1 lines in Zr, Nb and Pd are presented in Tables IV and V, respectively, and aluminumlike Pd^{33+} E1 transitions can be found in Table VI. (2-3 transitions in these three charge states in silver may be found in Ref.(2).) The observed Na-like lines are mostly within 1 mÅ of the calculated wavelengths, and as in the case of the F-like lines, there are many blends between adjacent transitions. The differences between the observed and calculated wavelengths are larger for the magnesiumlike ions than for the preceeding isosequences. The energy of the magnesiumlike $3s^2$ $J = 0$ ground state is sensitive to numerous small corrections from mixing with $J = 0$ levels of other even-parity configurations, up to and including levels in the continuum. Turning off all configuration interaction between $3s^2$ $J = 0$ and other $J = 0$ levels (particularly the two $3p^2$ $J = 0$ levels) increases the transition wavelengths (decreases the transition energies) for the lines in Table V by approximately 3 mÅ. For the observed Al-like Pd^{33+} lines, the wavelength difference with the calculations can be as large as 7 mÅ; in contra-distinction to the magnesiumlike case, this is

a result of incomplete accounting of the interaction between doubly excited states with inner-shell vacancies and the innershell-excited upper states listed in Table VI.

For higher n transitions in neonlike systems, the upper levels of certain lines in the $2p^6$ - $(2p^5)_{\frac{3}{2}}nd_{\frac{5}{2}}$ series and the $2p^6$ - $(2p^5)_{\frac{1}{2}}nd_{\frac{3}{2}}$ series can have nearly identical energies, giving rise to significant configuration interaction. In particular, the effect is seen in the enhancement of the intensity of the $2p^6$ - $(2p^5)_{\frac{3}{2}}7d_{\frac{5}{2}}$ transition at the expense of the $2p^6$ - $(2p^5)_{\frac{1}{2}}6d_{\frac{3}{2}}$ transition[10] in Mo^{32+}, where the difference in the upper state energy levels is 3.5 eV. A spectrum of these two lines is shown in Fig.4a. In the case of neonlike Nb^{31+}, the separation of these two lines is larger (7.1 eV), and the interaction is smaller, as seen in Fig.4b. The intensity of the $2p^6$ - $(2p^5)_{\frac{1}{2}}6d_{\frac{3}{2}}$ line has grown relative to the $2p^6$ - $(2p^5)_{\frac{3}{2}}7d_{\frac{5}{2}}$ line compared to the molybdenum case. For Zr^{30+}, the separation is 11 eV and there is little configuration interaction at all, as shown in Fig.4c. The smooth solid curves in Fig.4 are the synthetic spectra, and the relative intensities are proportional to the oscillator strengths. (See Table I.) This situation is somewhat muddled by the occurance of the sodiumlike 2p-8d transitions, shown by dotted lines in the figure. (See Table IV.) These observations are summarized in Fig.5 where the intensity ratios of the $2p^6$ - $(2p^5)_{\frac{3}{2}}7d_{\frac{5}{2}}$ and $2p^6$ - $(2p^5)_{\frac{1}{2}}6d_{\frac{3}{2}}$ lines are plotted as asterisks versus their upper energy level separation. The large error bar on the molybdenum point is due to the contribution from the unresolved sodiumlike line at 3141.4 mÅ. The solid circles are the calculated oscillator strength ratios as a function of calculated energy level separations, and the agreement is quite good. Also included are the calculated points from palladium, technetium, ruthenium and yttrium. In the case of Pd, Tc and Ru, the $2p^6$ - $(2p^5)_{\frac{1}{2}}6d_{\frac{3}{2}}$ line is at shorter wavelength and the $2p^6$ - $(2p^5)_{\frac{3}{2}}7d_{\frac{5}{2}}$ line is the *weaker* of the two.

The spectrum in the vicinity of the $2p^6$ - $(2p^5)_{\frac{3}{2}}nd_{\frac{5}{2}}$ series limit in Mo^{32+} was shown in Ref.(10), where transitions up to and including $2p^6$ - $(2p^5)_{\frac{3}{2}}18d_{\frac{5}{2}}$ were resolved, and the wavelength agreement with calculations was excellent. Spectra including the $2p^6$ - $(2p^5)_{\frac{3}{2}}nd_{\frac{5}{2}}$ series limit at 2914.78 mÅ, and the $2p^6$ - $(2p^5)_{\frac{1}{2}}nd_{\frac{3}{2}}$

series limit at 2841.44 mÅ in Mo^{32+} are shown in Fig.6. The wavelength calibration for these spectra was obtained from the high n series of hydrogenlike Ar^{17+}, transitions from 1s-5p to 1s-10p, with wavelengths of 2917.50, 2881.04, 2859.38, 2845.51, 2836.07 and 2829.36 mÅ[22]. The calculated $2p^6$ - $(2p^5)_{\frac{1}{2}}nd_{\frac{3}{2}}$ series[10] in Mo^{32+} with n between 10 and 19 is shown by the thick solid lines, and the 2s-7p and 2s-8p transitions are shown as the thin solid lines. This region of the spectrum is complicated by the presence of many Mo^{33+} transitions, shown as dotted lines. Clearly identified in the spectrum of Fig.6a are the Mo^{32+} $2p^6$ - $(2p^5)_{\frac{1}{2}}10d_{\frac{3}{2}}$ line at 2941.0 mÅ, the Mo^{32+} 2s-7p and 2s-8p lines at 2902.1 and 2853.0 mÅ, respectively (see Table II), the Mo^{33+} 2p-7d lines at 2935.8 mÅ, and the Mo^{33+} 2p-9d lines at 2930.2 mÅ and 2849.1 mÅ. Clearly missing from this spectrum are the transitions from the Mo^{32+} $2p^6$ - $(2p^5)_{\frac{1}{2}}nd_{\frac{3}{2}}$ series with n = 13, 14, 17, 18 and 19. The n = 11, 12, 15 and 16 lines have nearby transitions from Mo^{33+}, so the line identifications are ambiguous. The spectrum of Fig.6a was from a plasma with an electron temperature of 3.4 keV and an electron density of 7.7 x $10^{13}/cm^3$. At this temperature, Mo^{33+} is the dominant ionization state[34], so the presence of strong fluorinelike lines is expected. In contrast, shown in Fig.6b is a spectrum taken from a plasma with T_e = 2.1 keV and n_e = 8.8 x $10^{13}/cm^3$, where Mo^{32+} is the dominant charge state. In this spectrum, all of the Mo^{33+} lines have dropped in intensity, which suggests that the line at 2883.7 mÅ is due to 2p-8d Mo^{33+} transitions, and the lines at 2922.8, 2910.2 and 2878.6 mÅ, respectively, are the $2p^6$ - $(2p^5)_{\frac{1}{2}}11d_{\frac{3}{2}}$, $2p^6$ - $(2p^5)_{\frac{1}{2}}12d_{\frac{3}{2}}$ and $2p^6$ - $(2p^5)_{\frac{1}{2}}16d_{\frac{3}{2}}$ transitions.

Identifications of high n fluorinelike Mo^{33+} transitions are summarized in Table VII, where the upper levels, measured and theoretical wavelengths, and calculated oscillator strengths are given. A table of lower n Mo^{33+} lines can be found in Ref.(10). The $2p^6$ - $(2p^5)_{\frac{1}{2}}nd_{\frac{3}{2}}$ transitions with $n \geq 13$ (with the exception of $2p^6$ - $(2p^5)_{\frac{1}{2}}16d_{\frac{3}{2}}$) are missing from the spectra of Fig.6 because the upper states of these transitions lie above the ionization limit of the $2p^6$ - $(2p^5)_{\frac{3}{2}}nd_{\frac{5}{2}}$ series at 2914.78 mÅ, and the branching ratios towards autoionization is greater than 0.9 in every case. Radiative and autoionization rate coefficients for these levels are shown in

Fig.7. For all levels the autoionization rates are about a factor of 10 higher than the corresponding radiative rates, so it's reasonable that these lines are absent. From Fig.7 it is expected that the $2p^6$ - $(2p^5)_{\frac{1}{2}}12d_{\frac{3}{2}}$ transition would be supressed, but it is clearly visible in Fig.6. Given the very high accuracy of the energy level calculations for the neonlike and fluorinelike transitions in Tables I and VII (better than 1 part in 4000) it is unlikely that the first ionization potential for Mo^{32+} has been incorrectly calculated, so at present, no explanation is offered for why the $2p_{\frac{1}{2}}$ - $12d_{\frac{3}{2}}$ line is so strong. Similarly, the $2p^6$ - $(2p^5)_{\frac{1}{2}}16d_{\frac{3}{2}}$ transition is quite strong in Fig.6. It's possible that this upper level is selectively populated by charge exchange recombination.

For the higher temperature plasmas, molybdenum can reach the oxygenlike state[34]. The strongest 2p-4d transitions in Mo^{34+} are shown in Fig.8 and listed in Table VIII, dominated by the line at 3483.2 mÅ. Plasma parameters for the discharge for which this spectrum was obtained were T_e = 2700 eV and n_e = 9 x $10^{13}/cm^3$. In this spectral region under these conditions, five molybdenum charge states can be viewed simultaneously. O-like 2-3 transitions in barium may be found in Ref.(6).

Conclusions

X-ray transitions in the magnesiumlike through fluorinelike charge states in zirconium, niobium and palladium have been observed from Alcator C-Mod plasmas. Line identifications have been made by comparison to the results of *ab initio* calculations and overall wavelength agreement is very good. 2p-3d transitions in aluminumlike Pd^{33+} and 2p-4d transitions in oxygenlike Mo^{34+} have also been identified. The magnitude of the configuration interaction between the $(2p^5)_{\frac{1}{2}}6d_{\frac{3}{2}}$ level and the $(2p^5)_{\frac{3}{2}}7d_{\frac{5}{2}}$ level has been measured as a function of energy level spacing for the successive atomic number neonlike ions Mo^{32+}, Nb^{31+} and Zr^{30+}, and the agreement with theory is good. Transitions in the $2p_{\frac{1}{2}}$-$nd_{\frac{3}{2}}$ series in neonlike Mo^{32+}

with $n \geq 13$ are not observed, since the upper levels are greater than the ionization potential of the $2p_{\frac{3}{2}}$-$nd_{\frac{5}{2}}$ series, and autoionization to Mo^{33+} dominates over radiative transitions to the ground state.

Acknowledgements

The authors would like to thank F. Bombarda for assistance with the spectrometer system, U. Safronova for calculations of high n helium-like wavelengths, J. Irby for electron density measurements, A. Hubbard for electron temperature measurements and the Alcator C-Mod operations group for expert running of the tokamak. KBF would like to thank M.H. Chen for useful conversations and suggestions. Work supported at MIT by DoE Contract No. DE-AC02-78ET51013 and at LLNL by DoE Contract No. W-7405-ENG-48.

References

[1] E.Källne, J.Källne and R.D.Cowan, Phys. Rev. A **27**, 2682 (1983)

[2] P.Beiersdorfer et al., Phys. Rev. A **34**, 1297 (1986)

[3] P.Beiersdorfer et al., Phys. Rev. A **37**, 4153 (1988)

[4] E.V.Aglitskii et al., Physica Scripta **40**, 601 (1989)

[5] P.Beiersdorfer et al., Phys. Rev. Lett. **65**, 1995 (1990)

[6] R.Hutton et al., Phys. Rev. A **44**, 1836 (1991)

[7] M.B.Schneider et al., Phys. Rev. A **45**, R1291 (1992)

[8] Steven Elliott et al., Phys. Rev. A **47**, 1403 (1993)

[9] P.Beiersdorfer et al., Physica Scripta **51**, 322 (1995)

[10] J.E.Rice et al., Phys Rev A **51**, 3551 (1995)

[11] D.L.Matthews et al., Phys. Rev. Lett., **54**, 110 (1985)

[12] M.D.Rosen et al., Phys. Rev. Lett., **54**, 106 (1985)

[13] A.L. Osterheld et al., J. Quant. Spectrosc. Radiat. Transfer, **51**, No. 1/2, 263 (1994)

[14] P.Beiersdorfer, M.H.Chen, R.E.Marrs and M.Levine, Phys. Rev. A **41**, 3453 (1990)

[15] G.A.Chandler, M.H.Chen, D.D.Dietrich, P.O.Egan, K.P.Ziock, P.H.Mokler, S.Reusch and D.H.H.Hoffmann, Phys. Rev. A, **39**, 565 (1989)

[16] D.D.Dietrich, G.A.Chandler, P.O.Egan, K.P.Ziock, P.H.Mokler, S.Reusch and D.H.H.Hoffmann, Nucl. Instrum. Methods B, **24/25**, 301 (1987)

[17] E. Avgoustoglou, W.R. Johnson, Z.W. Liu and J. Sapirstein, Phys. Rev. A, **51**, 1196 (1995).

[18] W.R. Johnson, J. Sapirstein and K.T. Cheng, Phys. Rev. A, **51**, 297 (1995).

[19] M.Klapisch, Comput. Phys. Commun. **2**, 269 (1971)

[20] M.Klapisch, J.L.Schwob, B.S.Fraenkel and J.Oreg, J. Opt. Soc. Am. **67**, 148 (1977)

[21] P.J. Mohr, Phys. Rev. A, **26**, 2338 (1982) and references 1, 2 and 3 therein.

[22] I.H.Hutchinson et al., Phys. Plasmas **1**, 1511 (1994)

[23] M.A.Graf et al., Rev. Sci. Instrum. **66**, 636 (1995)

[24] J.E.Rice and E.S.Marmar, Rev. Sci. Instrum. **61**, 2753 (1990)

[25] G.W.Erickson, J. Phys. Chem. Ref. Data **6**, 831 (1977)

[26] E.S.Marmar et al., Phys. Rev. A **33**, 774 (1986)

[27] J.F.Seely and U.Feldman, Phys. Rev. Lett. **54**, 1016 (1985)

[28] L.A.Vainshtein and U.I.Safronova, Physica Scripta **31**, 519 (1985)

[29] U.I.Safronova, private communication (1995)

[30] L.W. Fullerton and G.A. Rinker, Phys. Rev. A, **13**, 1283 (1976).

[31] R.D.Cowan, The Theory of Atomic Structure and Spectra, University of California Press, pp.433-434 (1981)

[32] J. Oreg, W.H. Goldstein, M. Klapisch and A. Bar-Shalom, Phys. Rev. A **44**, 1750 (1991).

[33] J.E.Rice, E.S.Marmar, E.Källne and J.Källne, Phys. Rev. A **35**, 3033 (1987)

[34] K.B.Fournier et al., submitted to PRA (1995)

Table Captions

Table I Neonlike 2p-nl E1 transitions in Zr^{30+}, Nb^{31+} and Pd^{36+}. The upper level designations in the first column are indicated by three jj-coupled orbitals where '-' indicates $l - s$ coupling and '+' indicates $l + s$ coupling: the first two orbitals show the occupancy of the $2p_{\frac{1}{2}}$ and $2p_{\frac{3}{2}}$ subshells, respectively, the third orbital is where the 2p-electron has been promoted. It's the third orbital that makes the transition to fill the inner-shell vacancy. λ_E and λ_T are the experimental and theoretical wavelengths, respectively, and the g*fs are the calculated oscillator strengths. Also included is the 2p-3s transition in Pd^{36+}

Table II Neonlike 2s-np E1 transitions in Zr^{30+}, Nb^{31+}, Mo^{32+} and Pd^{36+}. The upper level designations in the first column are indicated by three jj-coupled orbitals where '-' indicates $l - s$ coupling and '+' indicates $l + s$ coupling: the first orbital shows the 2s-subshell vacancy, the second orbital indicates a full (spectator) 2p-subshell and the third orbital is where the 2s-electron has been promoted. The third orbital makes the transition to fill the inner-shell vacancy. The $2s_+[2p^6]6p_-$ J=1 transition in Mo^{32+}, shown by the asterisk, is at the same wavelength as the strong $2p^6$ - $(2p^5)_{\frac{3}{2}}12d_{\frac{5}{2}}$ transition in Mo^{32+} at 2986.4 mÅ.

Table III Fluorinelike E1 transitions in Zr^{31+} and Nb^{32+}. The upper level designations in the first column are indicated by three jj-coupled orbitals where '-' indicates $l - s$ coupling and '+' indicates $l + s$ coupling: the first two orbitals show the occupancy of the 2s and spectator or $2p_{\frac{1}{2}}$ and $2p_{\frac{3}{2}}$ subshells, respectively, and the third orbital is where the 2s- or 2p-electron has been promoted. The third orbital makes the transition to fill the inner-shell vacancy. The transition denoted (a) ends on the second excited state, $2s2p^6$ $J = 1/2$.

Table IV Sodiumlike E1 transitions in Zr^{29+}, Nb^{30+} and Pd^{35+}. The upper state of each transition is indicated by three jj-coupled orbitals where '-' indicates $l - s$ coupling and '+' indicates $l + s$ coupling: the first orbital is the inner shell vacancy (either 2s, $2p_{\frac{1}{2}}$ or $2p_{\frac{3}{2}}$), the second orbital is a spectator electron and

the third is the excited electron which makes the transition to fill the inner shell vacancy. The calculated $(2p_-)[3s]3d_-$ J=3/2 transition in Pd^{35+} (asterisk) is close in wavelength to the strong 2p-3d Pd^{36+} line at 3731.7 mÅ. The transitions denoted (a) end on the second excited state, $2p^6 3p\ J = \frac{3}{2}$. The transition denoted (b) ends on the first excited state, $2p^6 3p\ J = \frac{1}{2}$.

Table V Magnesiumlike 2p-nd E1 transitions in Zr^{28+}, Nb^{29+} and Pd^{34+}. The upper state of each transition is indicated by three *jj*-coupled orbitals where '-' indicates $l - s$ coupling and '+' indicates $l + s$ coupling: the first orbital is the inner shell vacancy (either 2s, $2p_{\frac{1}{2}}$ or $2p_{\frac{3}{2}}$), the second orbital lists the spectator electrons and the third is the excited electron which makes the transition to fill the inner shell vacancy. Also included are some 2s-3p transitions.

Table VI Aluminumlike Pd^{33+} E1 transitions. The upper state of each transition is indicated by three *jj*-coupled orbitals where '-' indicates $l - s$ coupling and '+' indicates $l + s$ coupling: the first orbital is the inner shell vacancy (either 2s, $2p_{\frac{1}{2}}$ or $2p_{\frac{3}{2}}$), the second orbital lists the spectator electrons and the third is the excited electron which makes the transition to fill the inner shell vacancy. The transitions denoted (a) end on the true ground state, $2p^6 3s^2 3p_-\ J = \frac{1}{2}$ and are enabled only through configuration mixing between the upper state and configurations of the form $\overline{2p}[3s^2 3p_-]3d_j\ J = \frac{3}{2}$ where $\overline{2p}$ indicates a hole in the 2p-subshell. The transition denoted (b) ends on the true ground state, $2p^6 3s^2 3p_-\ J = \frac{1}{2}$ and is enabled only through configuration mixing between the upper state and configurations of the form $\overline{2p}[3s^2 3p_-]3d_j\ J = \frac{1}{2}$. The transition denoted (c) ends on the first excited state, $2p^6 3s^2 3p_+\ J = \frac{3}{2}$.

Table VII High n fluorinelike Mo^{33+} E1 transitions. The upper level designations in the first column are indicated by three *jj*-coupled orbitals where '-' indicates $l - s$ coupling and '+' indicates $l + s$ coupling: the first two orbitals show the occupancy of the $2p_{\frac{1}{2}}$ and $2p_{\frac{3}{2}}$ subshells, respectively, the third orbital is where the 2p-electron has been promoted. The third orbital makes the transition to fill an inner-shell vacancy leaving the ion in the $2p^5\ J = \frac{3}{2}$ ground state. The calculated

2p-8d transitions around 2967.3 mÅ are nearly degenerate in wavelength with the strong $2p^6$ - $(2p^5)_{\frac{3}{2}}14d_{\frac{5}{2}}$ and $2p^6$ - $(2p^5)_{\frac{1}{2}}9d_{\frac{3}{2}}$ transitions in Mo^{32+}. Most of the observed lines are blends of two adjacent transitions.

Table VIII Oxygenlike Mo^{34+} E1 transitions. Transitions are indicated by both the upper and lower state. The index refers to the positions in the energy heirarchy of the nine levels possible from the $2s^22p^4$ ground configuration (5 levels) and the $2s2p^5$ first excited configuration (4 levels). Both lower and upper states are indicated by three jj-coupled orbitals where '-' indicates $l - s$ coupling and '+' indicates $l + s$ coupling: the first two orbitals show the occupancy of the 2s or $2p_{\frac{1}{2}}$ and $2p_{\frac{3}{2}}$ subshells, respectively, the third orbital is where the 2s- or 2p-electron has been promoted. The third orbital makes the transition to fill an inner-shell vacancy.

Table I Neon-like 2p-nl E1 Transitions

Upper level		Zr^{30+}			Nb^{31+}			Pd^{36+}	
	λ_E (mÅ)	λ_T (mÅ)	g*f	λ_E(mÅ)	λ_T (mÅ)	g*f	λ_E (mÅ)	λ_T (mÅ)	g*f
$(2p_-)(2p_+)^4 3s$ J=1		5609.5	.0851		5282.2	.0856	4001.4	4001.4	.0943
$(2p_-)^2(2p_+)^3 3d_+$ J=1		5375.0	1.776		5076.8	1.824	3904.7	3905.1	2.005
$(2p_-)(2p_+)^4 3d_-$ J=1		5199.0	1.741		4901.8	1.704	3731.7	3732.0	1.563
$(2p_-)^2(2p_+)^3 4d_+$ J=1		4195.2	.514	3958.3	3957.3	.515	3025.0	3025.9	.521
$(2p_-)(2p_+)^4 4d_-$ J=1	4079.6	4079.8	.309	3843.8	3842.8	.305	2914.0	2914.1	.289
$(2p_-)^2(2p_+)^3 5d_+$ J=1	3809.6	3808.8	.213	3591.2	3591.3	.213		2740.6	.213
$(2p_-)(2p_+)^4 5d_-$ J=1	3711.9	3710.9	.113	3494.7	3494.2	.112		2646.6	.106
$(2p_-)^2(2p_+)^3 6d_+$ J=1	3627.9	3627.7	.118	3420.2	3419.8	.118		2607.4	.118
$(2p_-)(2p_+)^4 6d_-$ J=1	3537.8	3537.8	.0446	3330.4	3330.8	.0414		2521.2	.0532
$(2p_-)^2(2p_+)^3 7d_+$ J=1	3526.8	3526.8	.118	3324.0	3324.2	.0887			
$(2p_-)(2p_+)^4 7d_-$ J=1		3441.2	.0364	3240.4	3239.5	.0352			
$(2p_-)^2(2p_+)^3 8d_+$ J=1		3464.6	.0460	3265.6	3265.3	.0459			
$(2p_-)(2p_+)^4 8d_-$ J=1		3381.6	.0253	3183.3	3183.1	.0249			
$(2p_-)^2(2p_+)^3 9d_+$ J=1		3423.1	.0401	3226.8	3226.1	.0399			
$(2p_-)(2p_+)^4 9d_-$ J=1		3341.9	.0187	3145.4	3145.6	.0187			
$(2p_-)^2(2p_+)^3 10d_+$ J=1				3200.8	3199.9	.0197			
$(2p_-)(2p_+)^4 10d_-$ J=1				3119.7	3120.4	.0103			
$(2p_-)^2(2p_+)^3 11d_+$ J=1				3178.5	3179.8	.0171			
$(2p_-)(2p_+)^4 11d_-$ J=1				3102.4	3101.3	.0076			
$(2p_-)^2(2p_+)^3 12d_+$ J=1				3163.3	3164.8	.0118			
$(2p_-)(2p_+)^4 12d_-$ J=1					3086.9	.0058			

Table II Neon-like 2s-np E1 Transitions

Jpper level		Zr^{30+}			Nb^{31+}			Mo^{32+}			Pd^{36+}	
	λ_E (mÅ)	λ_T (mÅ)	g*f	λ_E (mÅ)	λ_T (mÅ)	g*f	λ_E(mÅ)	λ_T (mÅ)	g*f	λ_E (mÅ)	λ_T (mÅ)	g*f
$2s_+[2p^6]3p_-$ J=1		4994.6	.102		4717.1	.105		4459.2	.108	3621.3	3619.0	.113
$2s_+[2p^6]3p_+$ J=1		4946.9	.310		4669.7	.311		4412.3	.312	3575.0	3572.8	.309
$2s_+[2p^6]4p_-$ J=1	3871.5	3868.7	.0438	3652.6	3649.9	.0441	3450.7	3449.3	.0445		2787.6	.0455
$2s_+[2p^6]4p_+$ J=1	3859.8	3856.8	.112	3640.5	3638.2	.110	3439.2	3437.7	.109		2776.3	.104
$2s_+[2p^6]5p_-$ J=1	3515.1	3514.0	.0167	3314.9	3314.1	.0167	3131.7	3130.7	.0162			
$2s_+[2p^6]5p_+$ J=1	3510.3	3509.3	.0442	3310.3	3309.3	.0436	3127.0	3126.0	.0431			
$2s_+[2p^6]6p_-$ J=1		3350.5	.0090	3163.3	3159.2	.0097	*	2983.9	.0098			
$2s_+[2p^6]6p_+$ J=1		3348.2	.0076	3158.5	3156.7	.0256	2982.4	2981.4	.0249			
$2s_+[2p^6]7p_-$ J=1								2902.7	.0057			
$2s_+[2p^6]7p_+$ J=1							2902.1	2901.4	.0143			
$2s_+[2p^6]8p_-$ J=1								2852.8	.0038			
$2s_+[2p^6]8p_+$ J=1							2853.0	2851.8	.0096			
$2s_+[2p^6]9p_-$ J=1								2819.8	.0027			
$2s_+[2p^6]9p_+$ J=1								2818.6	.0068			

Table III Fluorine-like E1 Transitions

Upper level		Zr^{31+}			Nb^{32+}	
	λ_E (mÅ)	λ_T (mÅ)	g*f	λ_E(mÅ)	λ_T (mÅ)	g*f
$2s[2p^5]_{3/2}4s_+$ J=3/2 (a)		4179.3	.0272	3942.4	3944.7	.0272
$(2p_-)^2(2p_+)^2 4s_+$ J=3/2		4137.2	.0444	3905.9	3906.0	.0443
$(2p_-)^2(2p_+)^2 4d_+$ J=1/2		4052.8	.102		3827.1	.102
$(2p_-)^2(2p_+)^2 4d_+$ J=3/2		4048.9	.343		3823.4	.344
$(2p_-)^2(2p_+)^2 4d_+$ J=5/2		4047.7	.664	3822.9	3822.3	.670
$(2p_-)(2p_+)^3 4d_+$ J=3/2		4035.1	.452		3810.8	.458
$(2p_-)^2(2p_+)^2 4d_+$ J=5/2		4020.9	.264	3800.0	3797.5	.265
$(2p_-)(2p_+)^3 4d_-$ J=5/2	3946.2	3946.4	.264	3718.2	3720.9	.261
$(2p_-)(2p_+)^3 4d_-$ J=1/2		3928.9	.171		3704.9	.171
$(2p_-)(2p_+)^3 4d_-$ J=3/2	3928.5	3928.1	.268	3704.4	3704.2	.269
$(2p_-)(2p_+)^3 4d_-$ J=5/2		3927.6	.208		3703.7	.270
$(2p_-)(2p_+)^3 4d_+$ J=5/2		3927.2	.104		3703.2	.0395
$2s[2p^5]_{3/2}4p_+$ J=3/2	3767.0	3764.4	.104	3555.3	3553.8	.103
$(2p_-)^2(2p_+)^2 5d_+$ J=3/2		3666.1	.168		3460.6	.168
$(2p_-)^2(2p_+)^2 5d_+$ J=5/2	3666.1	3665.7	.285	3460.3	3460.3	.284
$(2p_-)^2(2p_+)^2 5d_+$ J=5/2		3641.3	.0966	3439.3	3437.7	.0969
$(2p_-)(2p_+)^3 5d_-$ J=5/2	3582.0	3579.1	.108		3373.8	.107
$(2p_-)(2p_+)^3 5d_-$ J=3/2	3564.2	3564.2	.0924	3360.0	3360.2	.0931
$(2p_-)(2p_+)^3 5d_-$ J=5/2		3564.0	.0937		3360.1	.0951
$(2p_-)^2(2p_+)^2 6d_+$ J=3/2		3487.5	.0907		3291.5	.0908
$(2p_-)^2(2p_+)^2 6d_+$ J=5/2		3487.4	.154	3291.3	3291.4	.153
$(2p_-)^2(2p_+)^2 7d_+$ J=5/2		3388.1	.114		3197.3	.151

Table IV Sodium-like E1 Transitions

Upper level	Zr^{29+}			Nb^{30+}			Pd^{35+}		
	λ_E (mÅ)	λ_T (mÅ)	g*f	λ_E(mÅ)	λ_T (mÅ)	g*f	λ_E (mÅ)	λ_T (mÅ)	g*f
$(2p_+)[3s]3d_+$ J=3/2							3930.8	3930.0	2.074
$(2p_+)[3s]3d_+$ J=1/2							3918.6	3916.7	0.904
$(2p_-)[3s]3d_+$ J=3/2							3759.2	3758.1	1.135
$(2p_-)[3s]3d_-$ J=1/2							3756.7	3755.8	1.048
$(2p_-)[3s]3d_-$ J=3/2							*	3728.9	0.588
$2s[2p^6 3s]3p_+$ J=3/2							3601.9	3598.1	0.438
$(2p_-)[3p_+]4d_-$ J=5/2 (a)					4016.4	0.245		3064.5	0.285
$(2p_+)[3p_-]4d_+$ J=3/2 (b)				4014.2	4014.1	0.620		3062.8	0.643
$(2p_+)[3s]4d_+$ J=1/2		4254.8	0.300	4011.3	4012.0	0.302		3061.3	0.302
$(2p_+)[3p_+]4d_+$ J=1/2 (a)					4010.4	0.327		3060.3	0.334
$(2p_+)[3p_+]4d_+$ J=5/2 (a)					4010.3	0.471	3060.5	3060.3	0.494
$(2p_+)[3s]4d_+$ J=3/2		4251.2	0.611	4008.4	4008.6	0.614	3058.4	3058.9	0.613
$(2p_-)[3s]4d_+$ J=3/2		4135.5	0.044		3893.5	0.058		2945.3	0.138
$(2p_-)[3p_+]4d_-$ J=5/2 (a)					3893.3	0.364	2946.1	2946.7	0.368
$(2p_-)[3s]4d_-$ J=3/2		4133.6	0.322	3892.8	3891.9	0.306		2946.2	0.211
$(2p_-)[3s]4d_-$ J=1/2		4133.4	0.192		3891.9	0.190		2945.8	0.180
$(2p_+)[3s]5s$ J=3/2		3918.5	0.031		3693.2	0.046			
$2s[2p^6 3s]4p_+$ J=3/2		3901.0	0.105		3678.8	0.102			
$2s[2p^6 3s]4p_+$ J=1/2		3900.3	0.077		3678.2	0.080			
$2s[2p^6 3s]4p_+$ J=3/2		3886.9	0.043		3665.9	0.043			
$(2p_+)[3s]5d_+$ J=3/2		3875.4	0.041		3652.3	0.041			
$(2p_+)[3s]5d_+$ J=1/2		3874.5	0.019		3651.5	0.016			
$(2p_+)[3s]5d_+$ J=1/2	3872.7	3872.5	0.114	3649.8	3649.6	0.117			
$(2p_+)[3s]5d_+$ J=3/2	3871.0	3869.9	0.226	3647.4	3647.2	0.229			
$(2p_-)[3s]5d_+$ J=3/2	3770.3	3770.4	0.049	3548.8	3548.5	0.057			
$(2p_-)[3s]5d_-$ J=1/2		3769.7	0.073		3548.0	0.072			
$(2p_-)[3s]5d_-$ J=3/2		3769.6	0.080		3547.8	0.070			
$(2p_+)[3s]6d_+$ J=3/2		3696.3	0.039		3482.6	0.039			
$(2p_+)[3s]6d_+$ J=1/2		3695.4	0.055	3481.4	3481.8	0.054			
$(2p_+)[3s]6d_-$ J=1/2		3693.7	0.018		3480.2	0.019			
$(2p_+)[3s]6d_+$ J=3/2	3691.8	3691.9	0.109	3477.9	3478.6	0.109			
$(2p_-)[3s]6d_-$ J=3/2		3600.3	0.024		3387.4	0.060			
$(2p_-)[3s]6d_-$ J=1/2		3600.1	0.020	3386.4	3386.7	0.071			
$(2p_+)[3s]7d_+$ J=1/2	3594.6	3595.9	0.054		3388.5	0.001			
$(2p_+)[3s]7d_+$ J=3/2	3591.8	3592.7	0.070	3384.0	3384.5	0.085			
$2s[2p^6 3s]5p_+$ J=3/2		3561.6	0.038		3357.4	0.038			
$(2p_+)[3s]8d_+$ J=3/2		3535.1	0.021		3329.9	0.021			
$(2p_+)[3s]8d_+$ J=1/2	3533.4	3534.8	0.024	3328.4	3329.6	.0.25			
$(2p_-)[3s]7d_-$ J=3/2	3505.7	3505.3	0.021	3298.6	3298.0	0.024			
$(2p_-)[3s]7d_-$ J=1/2		3505.1	0.023		3297.8	0.014			

Table V Magnesium-like 2p-nd E1 Transitions

Upper level		Zr^{28+}			Nb^{29+}			Pd^{34+}	
	λ_E (mÅ)	λ_T (mÅ)	g*f	λ_E(mÅ)	λ_T (mÅ)	g*f	λ_E (mÅ)	λ_T (mÅ)	g*f
$(2p_+)[3s^2]3d_+$ J=1		5453.0	1.868		5148.5	1.918	3948.9	3950.3	2.102
$(2p_-)[3s^2]3d_-$ J=1		5271.9	1.755		4968.5	1.723	3774.6	3774.5	1.580
$(2s_+)[2p^6 3s^2]3p_+$ J=1		5023.4	0.295		4740.5	0.295	3621.3	3620.7	0.302
$(2p_+)[3s^2]4d_+$ J=1		4305.6	0.507		4058.3	0.509	3094.4	3092.1	0.514
$(2p_-)[3s^2]4d_-$ J=1		4184.0	0.296	3941.1	3937.8	0.293	2978.5	2975.9	0.280
$(2p_+)[3s^2]5d_+$ J=1	3934.5	3934.4	0.181	3705.5	3706.2	0.189		2816.2	0.199
$(2p_-)[3s^2]5d_-$ J=1	3835.3	3830.2	0.106	3603.0	3603.0	0.105		2717.4	0.100
$(2p_+)[3s^2]6d_+$ J=1	3760.4	3760.4	0.111	3543.5	3541.2	0.111		2687.2	0.112
$(2p_-)[3s^2]6d_-$ J=1		3664.5	0.001	3442.9	3445.6	0.086		2596.2	0.060
$(2p_+)[3s^2]7d_+$ J=1		3662.7	0.117	3445.1	3449.4	0.036		2615.4	0.060
$(2p_-)[3s^2]7d_-$ J=1		3571.2	0.031	3357.2	3358.1	0.031		2528.7	0.031

Table VI Aluminum-like Pd^{33+} E1 Transitions

Upper level	λ_E (mÅ)	λ_T (mÅ)	g*f
$(2p_+)[3s^2 3p_-]3d_+$ J=3/2	3983.7	3982.5	1.646
$(2p_+)[3s^2 3p_-]3d_+$ J=1/2	3980.2	3977.2	0.914
$(2p_+)[3s^2 3p_+]3d_-$ J=3/2 (a)		3972.7	0.262
$(2p_+)[3s^2 3p_+]3d_-$ J=1/2 (b)	3975.1	3971.3	0.446
$(2p_+)[3s^2 3p_+]3d_-$ J=3/2 (a)	3970.4	3963.4	0.341
$(2p_-)[3s^2 3p_-]3d_-$ J=3/2	3804.5	3804.6	1.360
$(2p_-)[3s^2 3p_-]3d_-$ J=1/2	3793.3	3792.1	1.011
$(2p_-)[3s^2 3p_-]3d_-$ J=3/2	3790.9	3784.1	0.526
$(2p_-)[3s^2 3p_+]3d_-$ J=5/2 (c)		3782.0	1.588
$2s_+[2p^6 3s^2 3p_-]3p_+$ J=3/2	3635.8	3641.1	0.358
$(2p_+)[3s^2 3p_-]4d_+$ J=3/2		3128.3	0.663
$(2p_+)[3s^2 3p_-]4d_+$ J=1/2		3128.0	0.334

Table VII Hign n Fluorine-like Mo^{33+} E1 Transitions

Upper level	λ_E (mÅ)	λ_T (mÅ)	g*f
$(2p_-)^2(2p_+)^27d_+$ J=3/2		3022.5	.0919
$(2p_-)^2(2p_+)^27d_+$ J=5/2	3022.3	3022.3	.182
$(2p_-)^2(2p_+)^28d_+$ J=1/2	*	2967.6	.0073
$(2p_-)^2(2p_+)^28d_+$ J=3/2	*	2967.3	.0328
$(2p_-)^2(2p_+)^28d_+$ J=5/2	*	2967.3	.0554
$(2p_-)^2(2p_+)^28d_+$ J=5/2		2948.8	.0169
$(2p_-)(2p_+)^37d_-$ J=5/2		2946.7	.0102
$(2p_-)(2p_+)^37d_-$ J=1/2		2936.2	.0044
$(2p_-)(2p_+)^37d_-$ J=3/2		2936.1	.0061
$(2p_-)(2p_+)^37d_-$ J=5/2	2935.8	2936.1	.0064
$(2p_-)^2(2p_+)^29d_+$ J=3/2		2930.8	.0223
$(2p_-)^2(2p_+)^29d_+$ J=5/2	2930.2	2930.7	.0380
$(2p_-)^2(2p_+)^29d_+$ J=5/2	2912.1	2912.5	.0108
$(2p_-)^2(2p_+)^210d_+$ J=3/2	2904.3	2905.2	.0190
$(2p_-)(2p_+)^38d_-$ J=5/2	2893.0	2894.3	.0223
$(2p_-)^2(2p_+)^210d_+$ J=5/2	2887.3	2887.2	.0082
$(2p_-)(2p_+)^38d_-$ J=1/2		2884.1	.0129
$(2p_-)(2p_+)^38d_-$ J=3/2	2883.7	2884.0	.0188
$(2p_-)(2p_+)^38d_-$ J=5/2		2884.0	.0176
$(2p_-)(2p_+)^39d_-$ J=5/2		2859.3	.0156
$(2p_-)(2p_+)^39d_-$ J=1/2		2849.3	.0080
$(2p_-)(2p_+)^39d_-$ J=3/2	2849.1	2849.3	.0119
$(2p_-)(2p_+)^39d_-$ J=5/2		2849.3	.0112
$(2p_-)(2p_+)^310d_-$ J=5/2		2834.9	.0116
$(2p_-)(2p_+)^310d_-$ J=3/2		2825.0	.0092
$(2p_-)(2p_+)^310d_-$ J=5/2		2825.0	.0091

Table VIII Oxygen-like Mo^{34+} E1 Transitions

Index	Lower level	Upper level	λ_E (mÅ)	λ_T (mÅ)	g*f
6	$2s(2p_-)^2(2p_+)^3$ J=2	$2s(2p_-)^2(2p_+)^2 4s$ J=2		3598.0	0.560
6	$2s(2p_-)^2(2p_+)^3$ J=2	$2s(2p_-)^2(2p_+)^2 4d_+$ J=3	3523.2	3522.4	0.652
6	$2s(2p_-)^2(2p_+)^3$ J=2	$2s(2p_-)^2(2p_+)^2 4d_+$ J=2		3521.4	0.482
2	$2s^2(2p_-)^2(2p_+)^2$ J=0	$(2p_-)^2(2p_+)4d_+$ J=1	3507.3	3507.8	0.249
4	$2s^2(2p_-)(2p_+)^3$ J=2	$(2p_-)(2p_+)^2 4d_+$ J=1		3490.5	0.179
1	$2s^2(2p_-)^2(2p_+)^2$ J=2	$(2p_-)^2(2p_+)4d_-$ J=1	3490.4	3489.8	0.037
4	$2s^2(2p_-)(2p_+)^3$ J=2	$(2p_-)(2p_+)^2 4d_+$ J=3		3488.7	0.710
1	$2s^2(2p_-)^2(2p_+)^2$ J=2	$(2p_-)^2(2p_+)4d_+$ J=2	3486.6	3485.4	0.276
1	$2s^2(2p_-)^2(2p_+)^2$ J=2	$(2p_-)^2(2p_+)4d_+$ J=3	3483.2	3481.7	0.900
3	$2s^2(2p_-)(2p_+)^3$ J=1	$(2p_-)(2p_+)^2 4d_-$ J=2		3479.5	0.039
3	$2s^2(2p_-)(2p_+)^3$ J=1	$(2p_-)(2p_+)^2 4d_-$ J=1	3478.2	3478.5	0.049
1	$2s^2(2p_-)^2(2p_+)^2$ J=2	$(2p_-)(2p_+)^2 4d_-$ J=2		3397.7	0.108
1	$2s^2(2p_-)^2(2p_+)^2$ J=2	$(2p_-)(2p_+)^2 4d_-$ J=3		3396.1	0.239
2	$2s^2(2p_-)^2(2p_+)^2$ J=0	$(2p_-)(2p_+)^2 4d_-$ J=1	3382.7	3382.1	0.274
1	$2s^2(2p_-)^2(2p_+)^2$ J=2	$(2p_-)(2p_+)^2 4d_-$ J=3		3380.6	0.339
1	$2s^2(2p_-)^2(2p_+)^2$ J=2	$(2p_-)(2p_+)^2 4d_-$ J=2	3380.3	3379.3	0.375
1	$2s^2(2p_-)^2(2p_+)^2$ J=2	$(2p_-)(2p_+)^2 4d_-$ J=1		3378.4	0.208

Figure Captions

Fig. 1 Plasma current, electron temperature, electron density and Pd x-ray (3.9-4.0 Å) brightness time histories in a discharge with a palladium injection at .5 sec.

Fig. 2 2p-3d transitions in Pd^{33+} - Pd^{36+}. Theoretical lines for neonlike Pd^{36+} (solid), Pd^{35+} (dotted), Pd^{34+} (dashed) and Pd^{33+} (dash-dot-dash) are shown at the bottom, where the relative intensities within a given charge state are proportional to the oscillator strengths of each transition.

Fig. 3 2p-5d transitions in neonlike Nb^{31+} (solid), Nb^{30+} (dotted) and Nb^{29+} (dashed), and 2s-4p transitions in Nb^{31+} (solid). Molybdenum transitions are shown by the thin dash-dot-dot-dot-dash lines.

Fig. 4 $2p_{\frac{3}{2}}$ - $7d_{\frac{5}{2}}$ and $2p_{\frac{1}{2}}$ - $6d_{\frac{3}{2}}$ transitions in the neonlike ions a.) Mo^{32+}, b.) Nb^{31+} and c.) Zr^{30+}, and the calculated neonlike (solid) and sodiumlike (dotted) lines.

Fig. 5 Ratios of the intensities of the $2p_{\frac{3}{2}}$ - $7d_{\frac{5}{2}}$ transitions to the $2p_{\frac{1}{2}}$ - $6d_{\frac{3}{2}}$ transitions as a function of the upper level energy differences are shown as asterisks for the observed lines. The calculated ratios of the oscillator strengths as a function of calculated energy differences are shown as solid dots. The points at -3.6, -9.0, -23.5 and +13.7 eV are for technetium, ruthenium, palladium and yttrium, respectively.

Fig. 6 Transitions in Mo^{32+} near the $2p_{\frac{1}{2}}$ - $nd_{\frac{3}{2}}$ series limit for a.) $T_e = 3400$ eV and b.) $T_e = 2100$ eV. Theoretical lines for Mo^{32+} (solid) and Mo^{33+} (dotted) are shown at the bottom, and the vertical dashed lines indicate the series limits. The molybdenum line at 2872.1 mÅ is unidentified.

Fig. 7 Autoionization and Einstein rate coefficients as a function of n for $2p_{\frac{1}{2}}$ - $nd_{\frac{3}{2}}$ transitions in Mo^{32+}.

Fig. 8 A spectrum including oxygenlike Mo^{34+}. Five molybdenum charge states are present in this figure, Mo^{34+} (thick dash-dot-dot-dot-dash lines) and Mo^{30+} - Mo^{33+} (thin dashed, dotted, solid and dash-dot-dash lines, respectively)[10].

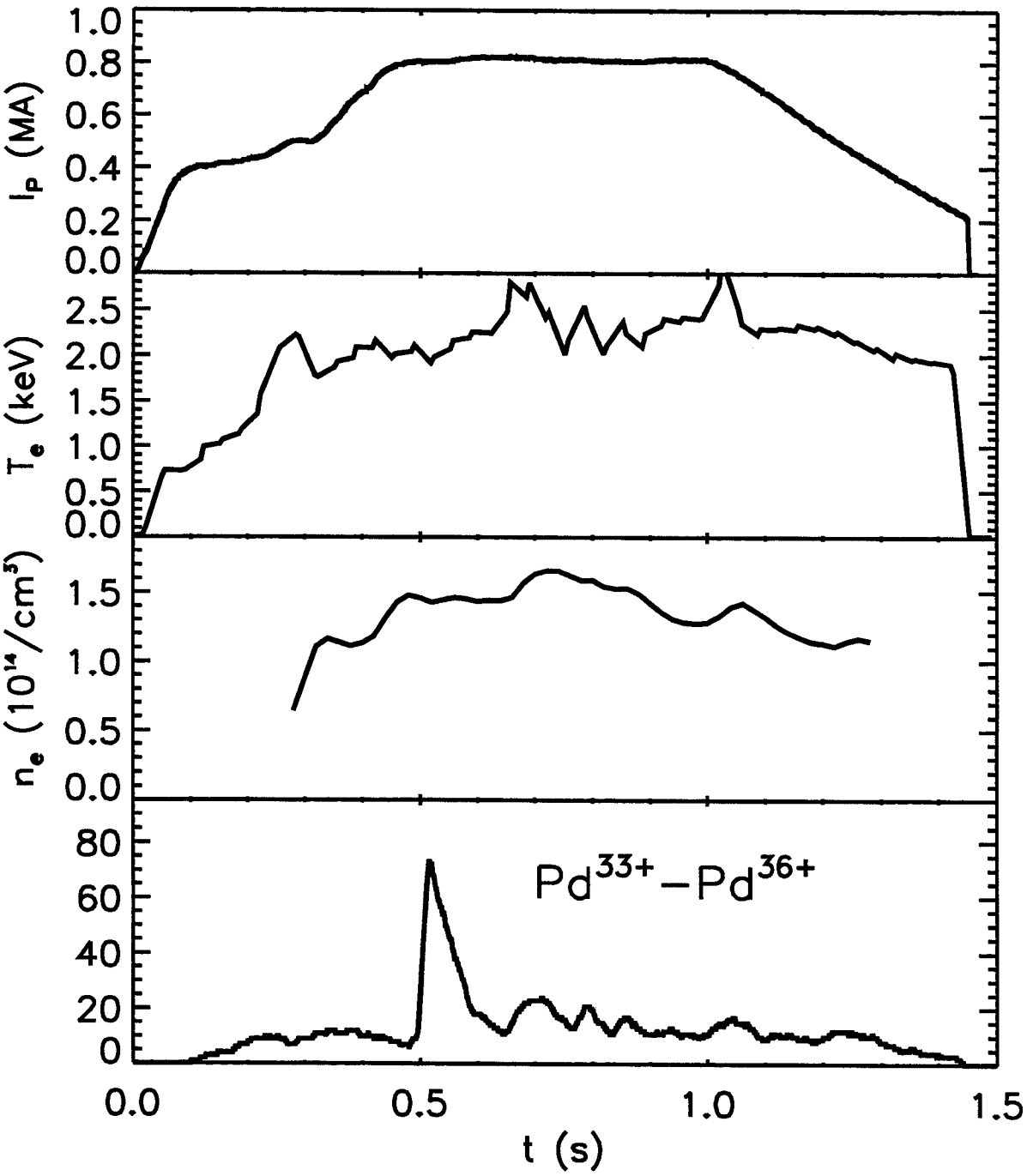
1.0
0.8
0.6
0.4
0.2
0.0
I_p (MA)
2.5
2.0
1.5
1.0
0.5
0.0
T_e (keV)
1.5
1.0
0.5
0.0
n_e (10^{14}/cm^3)
80
60
40
20
0
$Pd^{33+}-Pd^{36+}$
0.0
0.5
1.0
1.5
t (s)

Figure 1

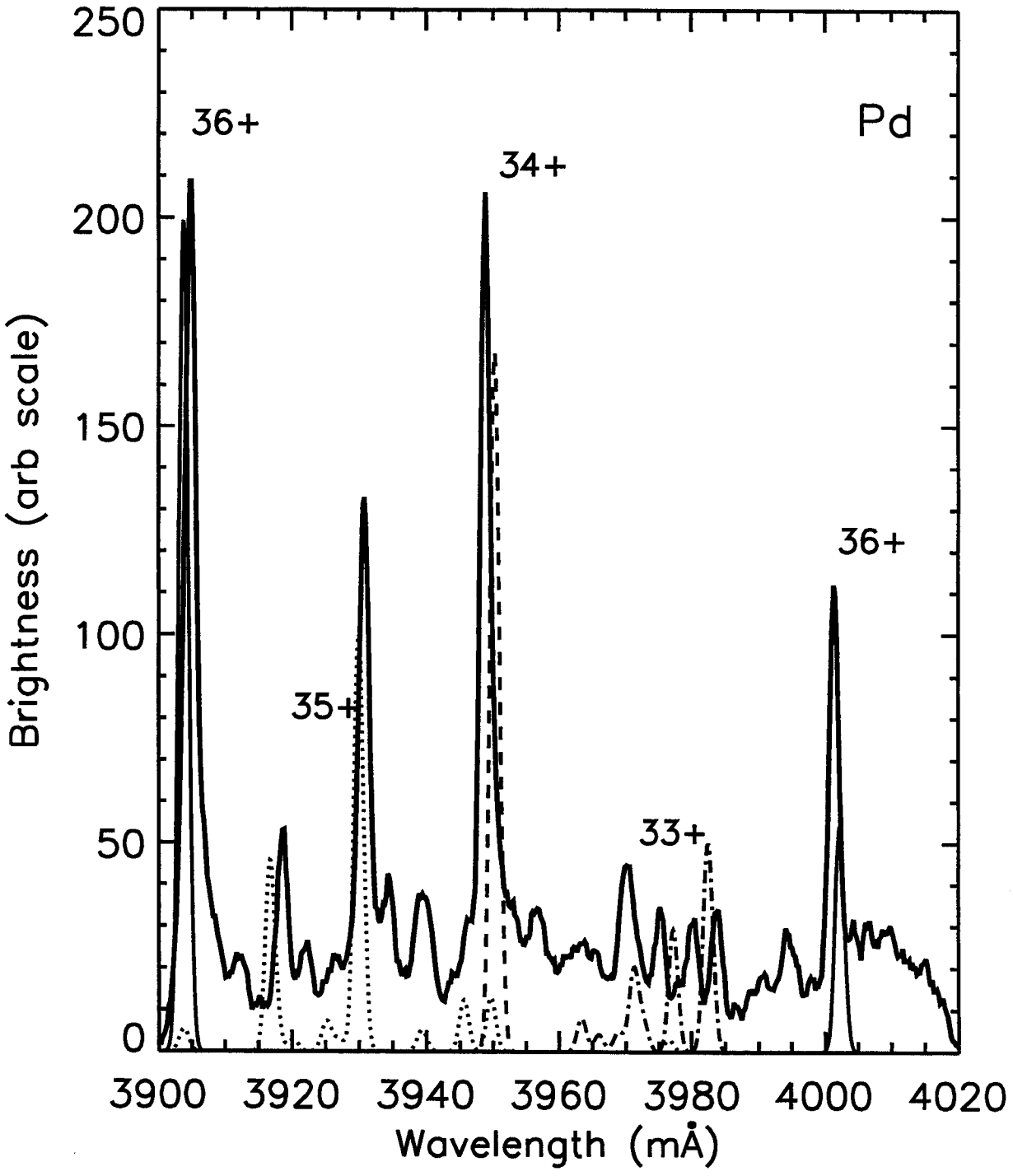
250
200
150
100
50
0
Brightness (arb scale)
36+
34+
35+
33+
36+
Pd
3900
3920
3940
3960
3980
4000
4020
Wavelength (mÅ)

Figure 2

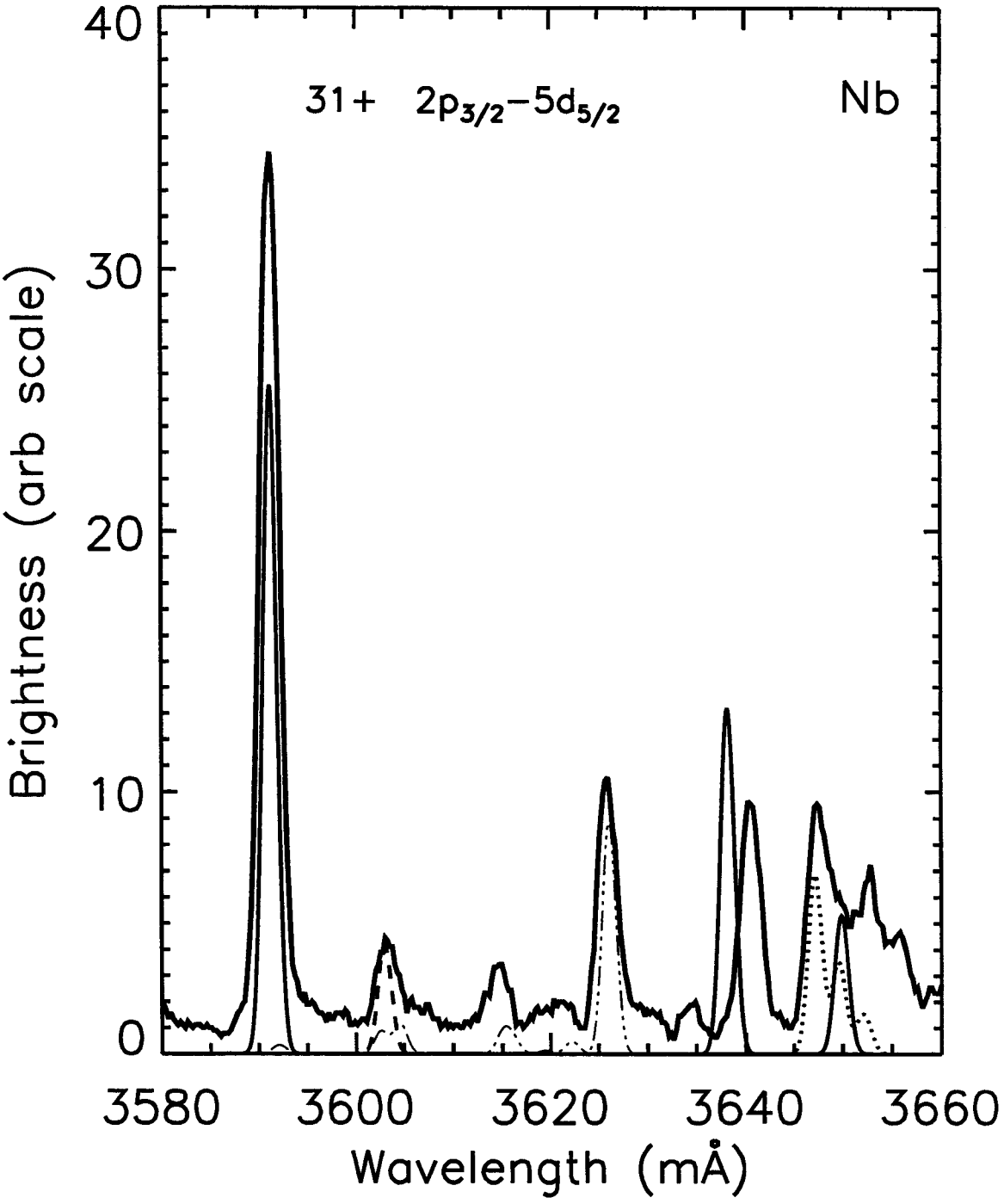
40
30
20
10
0
31+ $2p_{3/2}-5d_{5/2}$
Nb
Brightness (arb scale)
3580
3600
3620
3640
3660
Wavelength (mÅ)

Figure 3

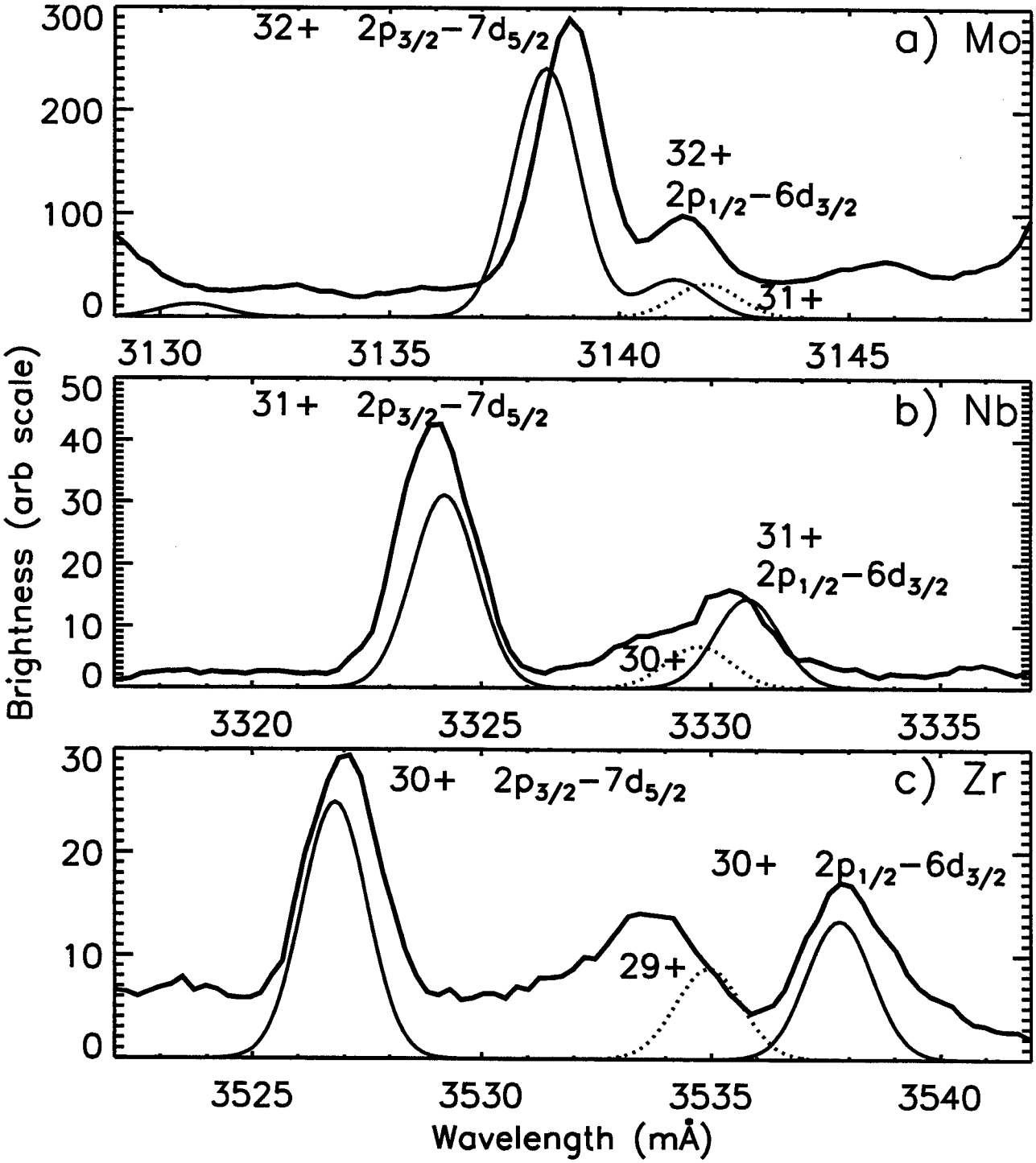
a) Mo
32+ $2p_{3/2}-7d_{5/2}$
32+ $2p_{1/2}-6d_{3/2}$
31+
b) Nb
31+ $2p_{3/2}-7d_{5/2}$
31+ $2p_{1/2}-6d_{3/2}$
30+
c) Zr
30+ $2p_{3/2}-7d_{5/2}$
30+ $2p_{1/2}-6d_{3/2}$
29+
Brightness (arb scale)
Wavelength (mÅ)

Figure 4

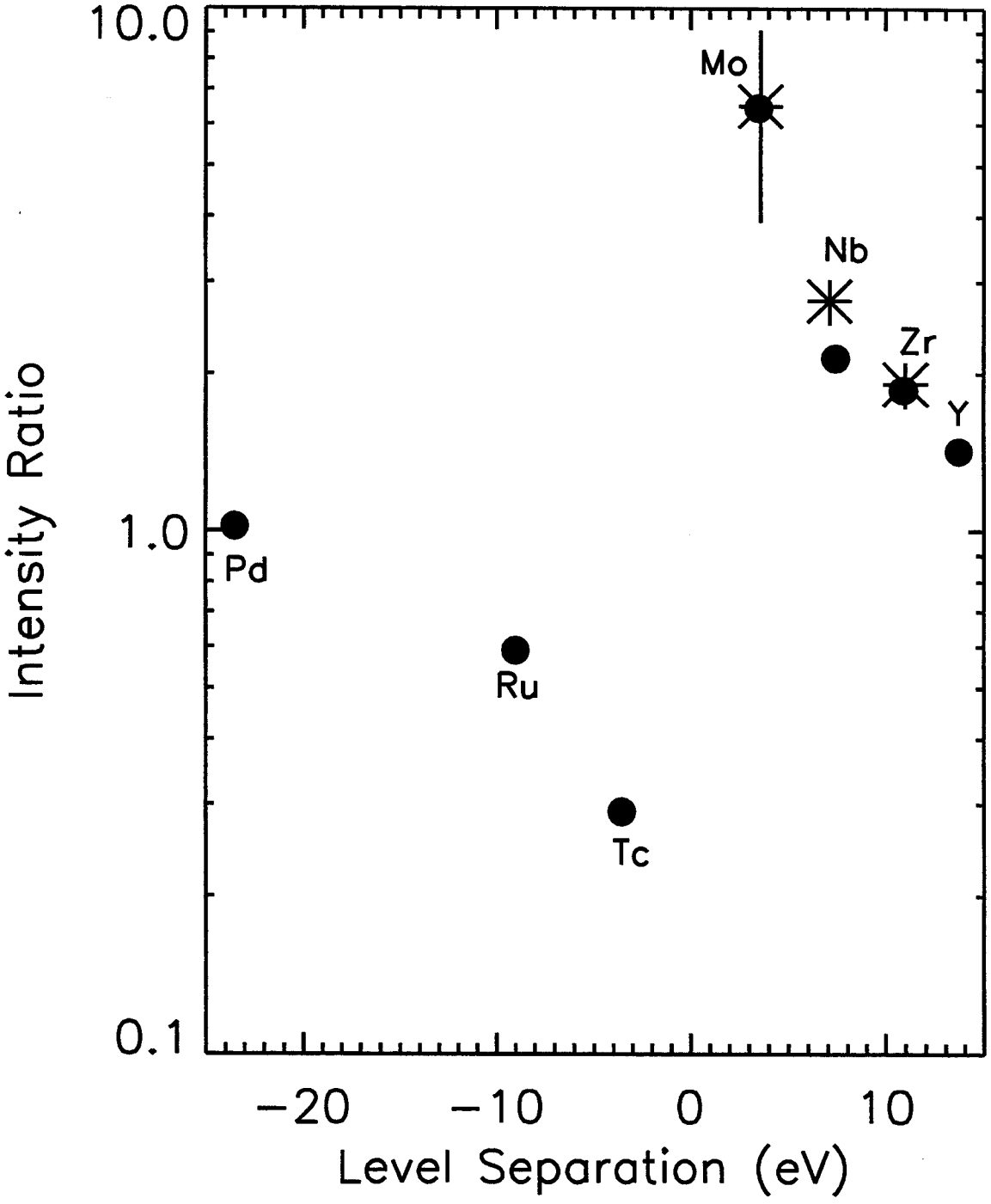
10.0
1.0
0.1
Intensity Ratio
Mo
Nb
Zr
Y
Pd
Ru
Tc
−20
−10
0
10
Level Separation (eV)

Figure 5

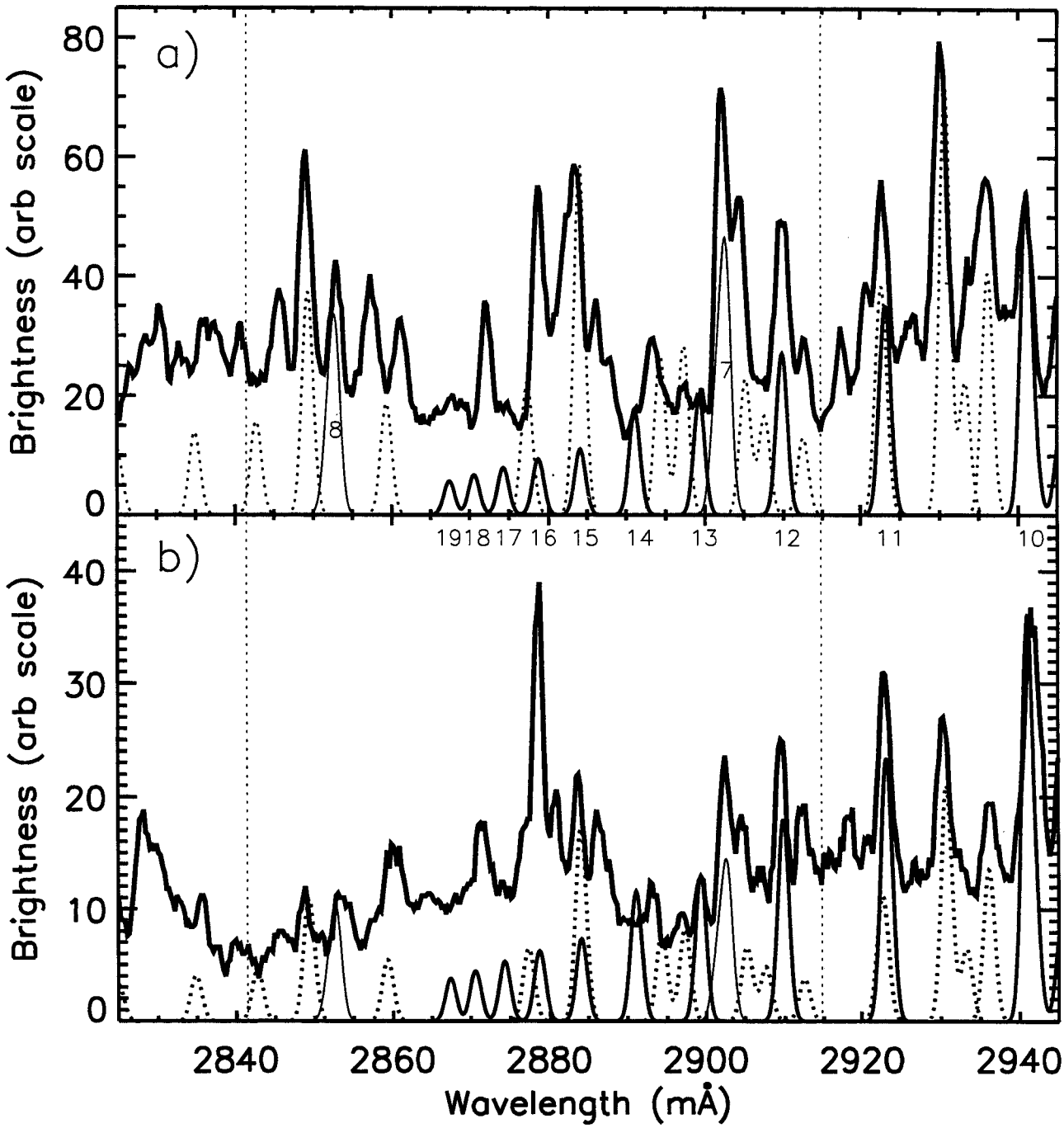
a)
b)
Brightness (arb scale)
Brightness (arb scale)
0
20
40
60
80
0
10
20
30
40
8
7
19 18 17 16 15 14 13 12 11 10
2840
2860
2880
2900
2920
2940
Wavelength (mÅ)

Figure 6

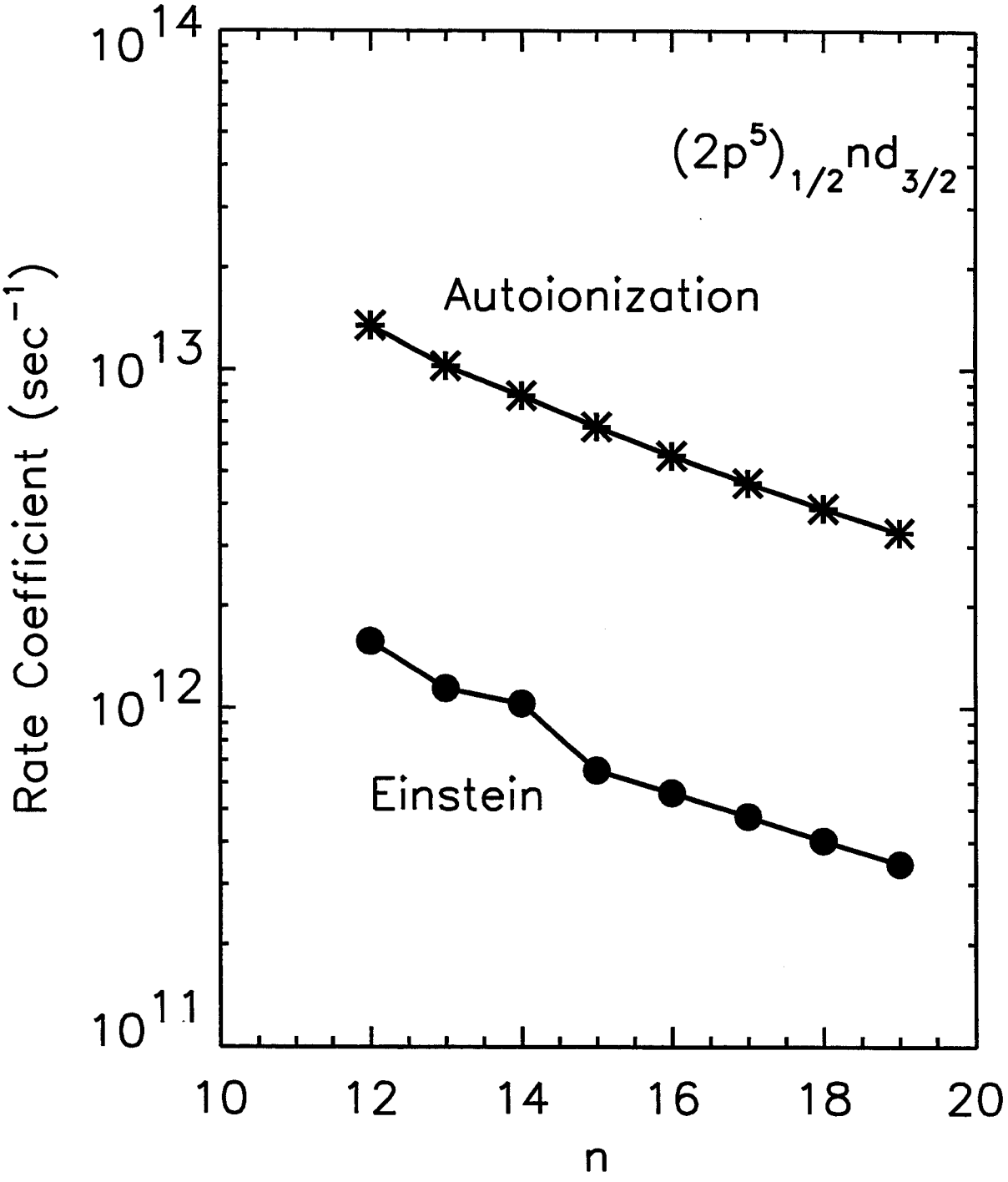
10^{14}
10^{13}
10^{12}
10^{11}
Rate Coefficient (sec^{-1})
$(2p^5)_{1/2}nd_{3/2}$
Autoionization
Einstein
10
12
14
16
18
20
n

Figure 7

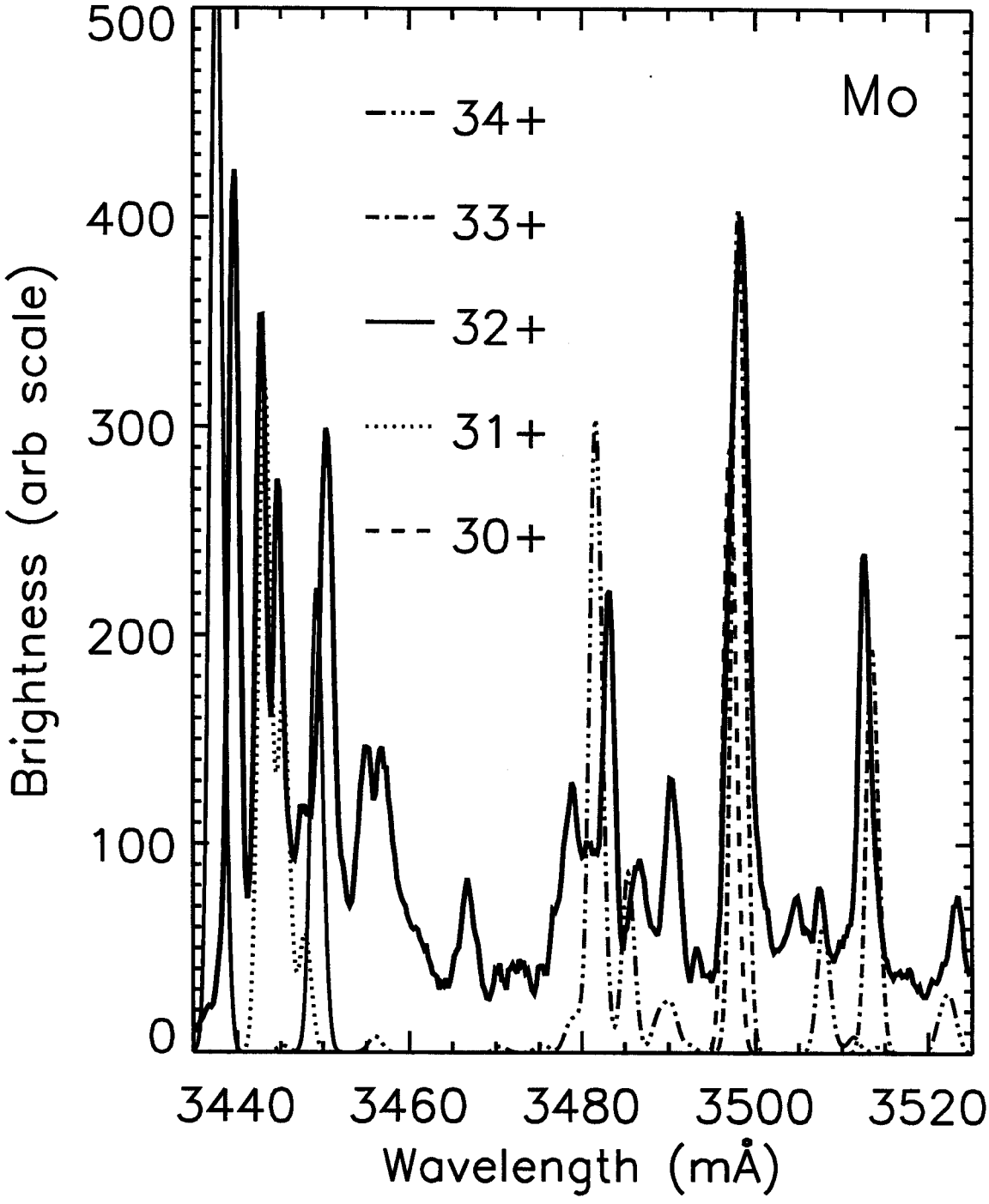
500
400
300
200
100
0
Brightness (arb scale)
34+
33+
32+
31+
30+
Mo
3440
3460
3480
3500
3520
Wavelength (mÅ)

Figure 8